New Journal of Physics
The open access journal at the forefront of physics

OPEN ACCESS

Superconducting complementary metasurfaces for THz ultrastrong light-matter coupling

To cite this article: Giacomo Scalari *et al* 2014 *New J. Phys.* **16** 033005

New Journal of Physics
The open access journal at the forefront of physics
Deutsche Physikalische Gesellschaft DPG | IOP Institute of Physics

Superconducting complementary metasurfaces for THz ultrastrong light-matter coupling

Giacomo Scalari[1], Curdin Maissen[1], Sara Cibella[2], Roberto Leoni[2], Pasquale Carelli[3], Federico Valmorra[4], Mattias Beck[4] and Jérôme Faist[4]

[1] Institute of Quantum Electronics, ETH Zürich, Switzerland
[2] CNR-IFN Rome, Italy
[3] DSFC, Università dell'Aquila, L'Aquila, Italy
[4] Institute of Quantum Electronics, ETH Zürich, Switzerland
E-mail: scalari@phys.ethz.ch

Received 2 November 2013, revised 5 February 2014
Accepted for publication 5 February 2014
Published 5 March 2014
New Journal of Physics **16** (2014) 033005
doi:10.1088/1367-2630/16/3/033005

Abstract

A superconducting metasurface operating in the THz range and based on the complementary metamaterial approach is discussed. Experimental measurements as a function of temperature and magnetic field display a modulation of the metasurface with a change in transmission amplitude and frequency of the resonant features. Such a metasurface is successively used in a cavity quantum electrodynamic experiment displaying ultrastrong coupling to the cyclotron transition of two-dimensional electron gas. A finite element modeling is developed and its results are in good agreement with the experimental data. In this system a normalized coupling ratio of $\frac{\Omega}{\omega_c} = 0.27$ is measured and a clear modulation of the polaritonic states as a function of the temperature is observed.

Keywords: metamaterial, superconductor, THz, ultrastrong, cyclotron

1. Introduction: ultrastrong light-matter coupling with THz metasurfaces and 2-dimensional electron gas

Light-matter interaction phenomena in a cavity lie at the heart of quantum photonics [1]. Recently, there has been considerable progress in the understanding and in the realization of

cavity-based light-matter coupling experiments covering a large portion of the electromagnetic spectrum, from the visible to the microwave range. When considering low-frequency photons, such experiments can benefit from the excellent characteristics of superconducting cavities which ensure low loss rates, allowing observation and manipulation of polaritonic systems, from atomic physics to solid state [2, 3].

Light-matter coupling in a cavity in solid state systems has been recently approaching a new regime, called ultrastrong coupling [4, 5], where the Rabi frequency of the system Ω is comparable to the bare excitation frequency of the matter part ω. In such a regime the system under consideration has to be treated beyond the rotating wave approximation, analogous to what happens in spin resonance for high irradiation powers leading to effects such as the Bloch–Siegert shift [6]. Semiconductor-based systems operating in the mid-IR [7–9] and THz [10–12] are particularly attractive for the study of this peculiar regime as very large intersubband dipole moments d can be achieved. The system can also benefit from the enhancement of the light-matter coupling by $\sqrt{N}$ deriving from the simultaneous coupling of N electrons to the cavity vacuum fluctuations E_{vac} of the same cavity mode. We recall that the r.m.s. vacuum field fluctuations at frequency ω_c are related to the cavity volume as $E_{vac} \sim \sqrt{\frac{\hbar\omega_c}{\varepsilon V_{cav}}}$, where V_{cav} is the cavity mode volume and $\varepsilon = n_{eff}^2$, where n_{eff} is the effective refractive index [13, 14]. In our *vacuum field* Rabi splitting experiments the average number of photons in the cavity is usually very small and the normal mode splitting is only due to the vacuum cavity field.

Ultrastrong coupling physics in the THz range has been also studied and experimentally realized without a cavity by intense THz irradiation of semiconductor quantum wells [15, 16]. This high field regime leads to the observation of phenomena such as Autler–Townes splitting and Bloch–Siegert shift.

We recently demonstrated that the cyclotron transition of a 2-dimensional electron gas (2DEG) coupled to a metasurface of subwavelength split-ring resonators can attain the ultrastrong coupling regime showing record high values of the normalized light-matter coupling ratio $\frac{\Omega}{\omega_c} = 0.58$ [17, 18]. As discussed in the introduction of the work of Hagenmüller *et al* [14], starting from the constitutive relation $\hbar\Omega = d \times E_{vac} \times \sqrt{N}$ and using the same symbols it can be shown that the normalized light-matter coupling ratio $\frac{\Omega}{\omega_c}$ for this cyclotron-based system scales in the following way with the relevant physical parameters:

$$\frac{\Omega}{\omega_c} \sim \underbrace{el_0\sqrt{\nu}}_{\text{dipole}} \times \underbrace{\frac{\sqrt{\frac{1}{\hbar\omega_c\varepsilon\varepsilon_0 L_z S}}}{E_{vac}/\hbar\omega_c}}_{} \times \underbrace{\sqrt{\frac{\rho_{2DEG} n_{QW}}{\nu}}}_{\text{collective enhancement}}. \tag{1}$$

Here $\nu = \frac{2\pi\hbar\rho_{2DEG}}{eB}$ is the 2DEG fill factor (with ρ_{2DEG} sheet electronic density and e the absolute value of the elementary charge), n_{QW} is the number of 2DEGs in the cavity, $l_0 = \sqrt{\frac{\hbar}{eB}}$ is the magnetic length, $V_{cav} = L_z S$ where L_z is the extension of the cavity mode in the direction parallel to the static magnetic field B and S is the mode extension in the plane of the 2DEG.

By exploiting the detailed calculations of [14] we can write an expression for the coupling ratio of the system as:

$$\frac{\Omega}{\omega_c} = \sqrt{\frac{\lambda}{L_z}\frac{\alpha n_{QW}\nu}{4\pi^2\varepsilon\varepsilon_0}} \tag{2}$$

where $\alpha = \frac{e^2}{\hbar c}$ is the fine structure constant and λ is the wavelength (in vacuum) of the THz field. Equation (2) highlights the dependence on $\sqrt{\nu}$ as well as on the ratio between the wavelength and the cavity thickness $\sqrt{\frac{\lambda}{L_z}}$.

This fully tunable system is very promising for the study of ultrastrong light-matter physics since the coupling ratio scales with the filling factor ν. This means that as long as the cyclotron transition can be resolved, the experiments can be scaled down in frequency, achieving coupling ratios in principle much higher than unity [14]. The ultrastrong coupling regime of cavity QED has been predicted to display intriguing and peculiar quantum electrodynamics features: Casimir-like [19] squeezed vacuum photons upon either non-adiabatic change or periodic modulation in the coupling energy [4], non-classical radiation from chaotic sources [20], ultrafast switchable coupling [21] and spontaneous conversion from virtual to real photons [22].

The paper is organized as follows: in section 2 we present the metasuface design and its fabrication. In sections 2.1 and 2.2 we analyze the behavior of the metasurface as a function of the temperature and of the applied magnetic field respectively, together with finite element modeling. In section 3 we then present the measurements and modeling of the Nb metasurface strongly coupled to the cyclotron transition of a 2DEG.

2. The metamaterial cavity: fabrication, experimental results, and modeling

In our previous experiments [17, 18], we employed metasurfaces of split-ring resonators that, when probed in transmission, show an absorption dip at the resonant frequency of the LC mode. The characteristic anticrossing behavior of the polaritonic system is probed by scanning the magnetic field. This provides a linear tuning of the cyclotron energy. With such an experimental arrangement we have observed three absorption features [17, 18]: two are related to the light-matter coupled system and the third middle peak is the cyclotron signal coming from the material which lies in between the resonators. This cyclotron signal is only weakly coupled to the metasurface and follows the expected linear dispersion for a cyclotron transition $\hbar\omega_c = \frac{\hbar eB}{m^*}$. In order to observe with greater detail the spectroscopic features of the polaritonic branches, we now change the configuration of the metamaterial cavity and employ a complementary cavity.

As already shown in several papers [23, 24], the complementary metamaterial is obtained by exchanging the roles of the vacuum areas and of the metals composing the metasurface. The resulting metasurface is constituted of a metallic sheet with openings in the shapes of the resonators. When excited with an electric field perpendicular to the one used in the case of the direct metamaterial (i.e. along the y axis, perpendicular to the central gap as in figure 1(c)), the resonator will display a transmission spectrum which is complementary to the one shown by the split ring resonators (i.e. transmission peaks instead of transmission dips [24]).

The intriguing quantum optical predictions for an ultrastrongly coupled system rely on a non-adiabatic modulation [4, 8, 19] of the system's parameters, in our case on timescales shorter than the inverse of the Rabi frequency of the system (10–2.5 ps). The fabrication of a superconducting cavity offers an interesting opportunity in this direction, since the cavity

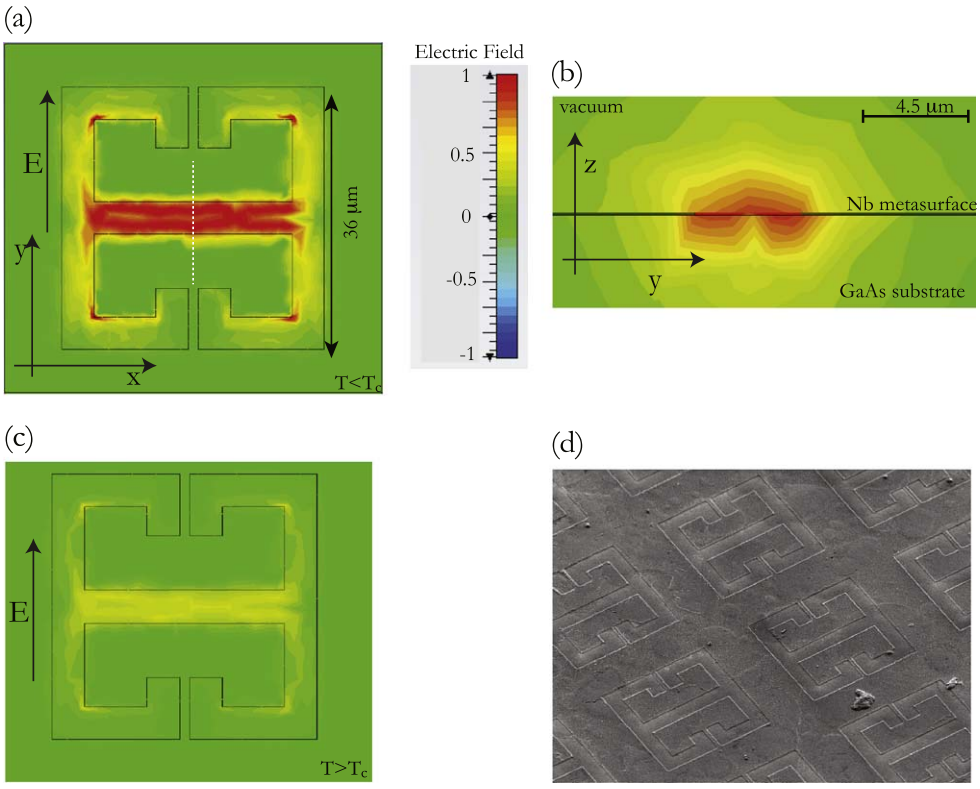

Figure 1. (a) In-plane electric field $E_{plane} = \sqrt{E_x^2 + E_y^2}$ for the resonator operating at 440 GHz. The simulation is performed with CST microwave studio, by sending a plane wave orthogonal to the plane of the metasurface and with the electric field polarization parallel to the *y*-axis. The Nb is in the superconducting state, and is simulated using the measured values for the superconductor complex surface impedance, reported in figure 2(b). (b) In-plane electric field distribution in the y–z plane following the white dashed line of panel (a). (c) In-plane electric field intensity for the resonator operating in the normal state. (d) SEM picture of the fabricated sample with 100 nm-thick Nb metasurface on top of the 2DEG.

characteristics strongly depend on the state, superconducting or normal, in which the material operates. On the other hand, even if in our case the quality factor of the split-ring resonator is radiatively limited, the presence of the superconductor will mitigate the ohmic losses, yielding a longer polariton coherence time. In the last few years many examples of superconducting GHz and THz metamaterials have been presented, both using BCS superconductors like Nb and NbN [25–27], or dealing with high T_c superconductors [28]. For our cavity we chose Nb, which is a well-known superconducting material widely employed in THz science. The niobium film of the resonators, about 100 nm thick, is deposited by dc-magnetron sputtering both on a semi-insulating (SI) GaAs (for the control sample) and on a sample containing a triangular well 2DEG (for the strong-coupling experiment). On top of the Nb film we spun an electronic resist (Polymethyl Methacrylate, positive tone electronic resist), and the pattern was defined by direct writing with electron beam lithography. Successively, the niobium was selectively removed by means of a dry reactive ion etching. A scanning electron microscope picture of the fabricated devices is presented in figure 1(d). The Nb film has a critical temperature T_c of 8.7 K, as results

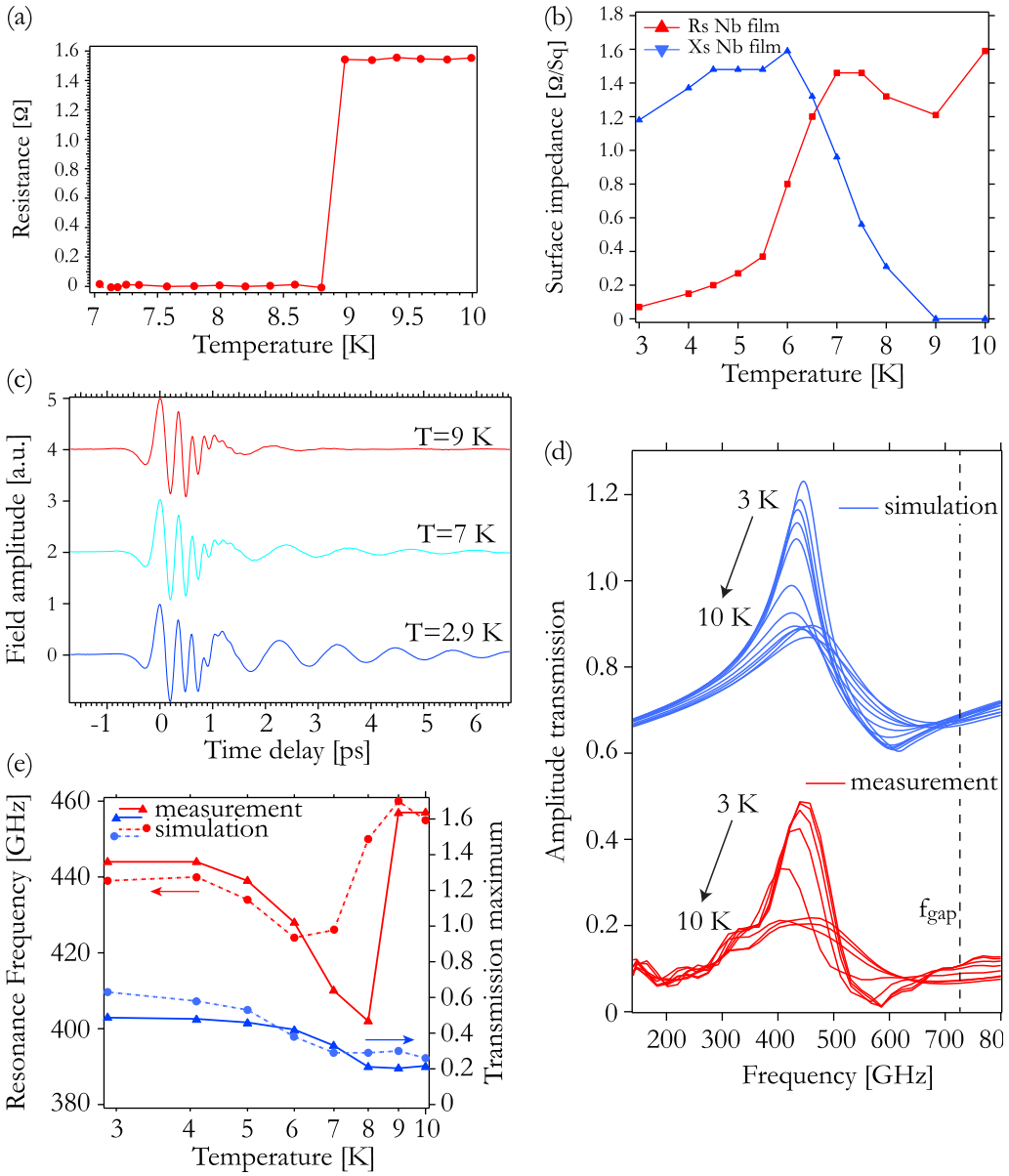

Figure 2. (a) DC resistance measurement as a function of the temperature for the 100 nm-thick Nb film used to fabricate the metasurface. (b) Measured complex surface impedance at the frequency of 440 GHz for the Nb film as a function of temperature. (c) Electric field magnitude as a function of time of the THz-TDS signal transmitted through the metasurface and deposited on SI GaAs for three different temperatures. (d) Simulated (top) and measured (bottom) transmission for the superconducting metasurface deposited on the SI GaAs as a function of the temperature varied in the range 2.9–10 K. The simulated curves are offset by 0.6 for clarity. The surface impedance values $Z_s = R_s + iX_s$ are extracted from the conductivity measurement of the Nb film reported in panel (b) of this figure. (e) Measured (triangles) and simulated (circles) transmission peak and frequency as a function of the temperature for the Nb metasurface.

from DC resistance measurements reported in figure 2(a). From this T_c value we can infer a gap value of $E_g = 2\Delta = 4.1 K_B T_c \simeq 3$ meV which corresponds to $f_{gap} \simeq 730$ GHz [29].

In figure 1(a) we present the design of our resonator (very similar to the one proposed in [24]) and the in-plane electric field distribution (which is the one relevant for the inter-Landau level coupling) for the LC resonance when the superconductor is in the superconducting state. The simulation is performed with CST microwave studio, by sending a plane wave orthogonal to the plane of the metasurface and with the electric field polarization parallel to the *y*-axis (black arrow in figures 1(a), (c)). Further details about the modeling of the metasurface wil be given in section 2.1. The capacitor, where the majority of the electric field is concentrated, is constituted by the central section of the resonator of width 4.5 μm and effective length 27.5 μm. The effective volume of the cavity in this case can be estimated as $V_{cav} = L_z \times S \simeq 3.2 \times (27.5 \times 4.5) \times 10^{-18} = 8.6 \times 10^{-16}\,\mathrm{m}^3$ which yields a ratio of $\frac{V_{cav}}{(\lambda / 2n_{eff})^3} \simeq 1 \times 10^{-3}$.

In figure 1(c) we plot the in-plane electric field distribution simulated with the superconductor in the normal state: the electric field enhancement results are approximately one half of the one simulated for the superconducting case.

2.1. THz metasurface characteristics as a function of the temperature

The complementary metasurface, first fabricated on SI GaAs, is then probed with THz-time domain spectroscopy (TDS) in a range of temperatures above and below T_c. The experimental setup employed in this paper is based on a THz-TDS system coupled to a split-coil superconducting magnet and is described in detail in [17, 18] As visible from figures 2(c)–(e), a clear change in the metasurface quality factor Q and a shift of the resonance frequency are observed between 8 K and 9 K, as already observed in direct metamaterials fabricated with other kind of superconductors [28]. The deduced high-frequency T_c of 8.5 K is in good agreement with the DC value and the one found in similar structures [26].

The observed behavior of the superconducting complementary metasurface can be explained by considering the complex conductivity of the metasurface and the LC nature of the resonance. For a superconductor like Nb in the normal state (above T_c) the conductivity σ is essentially real and in thin films was found in the range of $\sigma_{T>T_c} = 2.5 \times 10^7 \mathrm{Sm}^{-1}$ [29]. Below T_c, σ is mainly complex and frequency dependent: the complex part displays low values in proximity to the superconducting gap frequency f_{gap}. In order to model the system we can proceed following Chen *et al* [28] by considering that the surface impedance of a superconducting film with a thickness D can be expressed as $Z_s = R_s + iX_s = \sqrt{\frac{i\omega\mu_0}{\sigma}}\, Coth\,(D\sqrt{i\omega\mu_0\sigma})$ where σ is the complex conductivity. The resistive part R_s and the reactive part X_s can then be connected to the parameters of the resonator, seen as an RLC circuit.

Still along the analysis presented in [28] we can express the resonance of the LC mode in the following way:

$$\nu_{res} = \frac{1}{2\pi}\sqrt{\left(\frac{1}{(L_g + L_k)C} - \frac{R^2}{4(L_g + L_k)^2}\right)} \tag{3}$$

where L_g is the geometrical value of the inductance, L_k represents the kinetic inductance due to the imaginary part of the conductivity, and R is the resistance of the circuit, related to the real part of σ. When the temperature is above T_c, the value of L_k is extremely small and the resistance R is inversely proportional to the real part of the Nb conductivity. The shift of the resonance for temperatures just below T_c is mainly due to the emergence of the imaginary part of the conductivity which effectively introduces the kinetic inductance of the Cooper pairs. Across the superconducting transition, we will have the value of R that will change due to the change of the real part of the conductivity and the reactive part which will become relevant as it introduces a supplementary term $L_k(X_s)$ which effectively lowers the frequency. This explains the redshift of the resonance between 9 K and 7 K. Further reduction of the temperature increases the imaginary conductivity and also reduces the resistance term R. This is reflected in two aspects: a narrowing of the resonance due to reduced dissipation and a blue shift due to the reduction of R, which restores a higher value for the resonance frequency (the rightmost term under square root in equation (3) is responsible for this behavior).

We measured the complex conductivity of the employed 100 nm–thick Nb unstructured film as a function of the temperature with THz-TDS. Successively we calculated the complex surface impedance and we extracted the values at the resonant frequency f = 440 GHz. These values are reported in figure 2(b) and then used to perform the 3D calculation. As visible from figures 2(d) and (e), the experimental results are well reproduced by the 3D modeling performed with CST microwave studio using a surface impedance model (ohmic sheet) for the superconductor. We performed a frequency domain simulation with a meshing accuracy of 10^{-5} in the frequency range 50–1700 GHz. The small discrepancy between the simulated amplitude transmission and the measured one has already been observed in similar experiments [28] and can be ascribed to different causes. We believe the main reason is that the values for the complex conductivity are considered as frequency independent in the simulations: this is not true, as they present quite large variations, especially when approaching the gap frequency: our resonator is in fact operating slightly below the gap frequency ($\nu_{res} = 440$ GHz $< f_{gap} = 730$ GHz) and this simplification can explain the semi-quantitative agreement between simulations and experiments. As already observed in [29], we report an enhanced transmission for frequency above f_{gap}.

2.2. THz metasurface characteristics as a function of perpendicular magnetic field

In order to model the complete system when the 2DEG is coupled to the resonator and measured as a function of the magnetic field, we need to study and model the resonator behavior also as a function of the applied magnetic field. We now analyze the data of the superconducting metasurface deposited on top of SI GaAs at a temperature of 2.9 K subjected to a perpendicular magnetic field of increasing strength. The measured transmission spectra are reported in figure 3(a) (red traces). The application of a perpendicular magnetic field leads to a steady decrease of the transmission at resonance and a slight redshift up to a field value of 1.5 T. At this point a transition occurs and the resonator linewidth broadens considerably together with a blueshift of the resonant frequency: this shape and both the transmission value and the

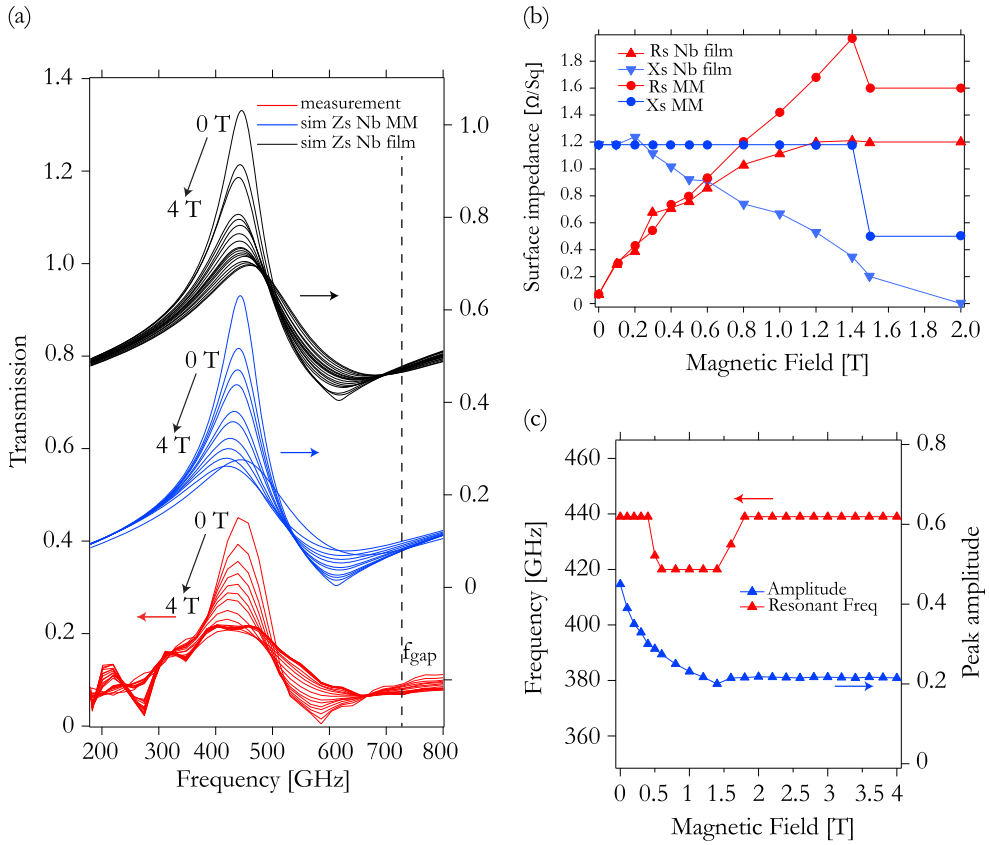

Figure 3. (a) Simulated (top, black and blue) and measured (bottom) transmission for the superconducting metasurface fabricated on the SI GaAs as a function of the magnetic field at a temperature of 2.9 K. Black curves are offset by 0.4 for clarity. The surface impedance values labeled 'Z_s Nb' film are extracted from the conductivity measurement of the Nb film reported in panel (b) of this figure. (b) Measured complex surface impedance at the frequency of 440 GHz for the Nb film as a function of the applied magnetic field (points labeled 'Nb film'). (c) Measured peak amplitude and resonant frequency for the Nb metasurface as a function of magnetic field at T = 2.9 K.

resonant frequency stay constant until high values of the applied magnetic field (see figure 3 (c)) are reached.

In a type II superconductor such as Nb, the application of a perpendicular magnetic field produces current vortices in the sample which surround regions of normal state conductivity, where the magnetic field can penetrate the sample [30–32]. At the same time, there is an increasing portion of the sample which presents normal state for Nb, and these two effects enter in a non-trivial way into the expression for the surface impedance. The plain Nb film was measured this time as a function of the magnetic field at a constant temperature of T = 2.9 K. The extracted surface impedance at 440 GHz is reported in figure 3(b) and is used to model the resonator. The results are reported in figure 3(a) as black lines: the change in transmittance is well reproduced but the frequency shift shows an opposite behavior. In order to get useful parameters to use in the simulation of the complete system, we use effective values for the metasurface complex impedance parameter, seeking the best agreement between simulation and experimental data. These parameters are reported in figure 3(b) and labeled as 'R_s MM' and

'X_s MM' and are effective values for the metamaterial. The results of the simulations with such parameters are reported in figure 3(a) (blue lines). In order to reproduce the experimental results, we need to keep the reactance value X_s constant until the critical field value of 1.5 T is reached and change only the resistive part. This behavior, which differs from what was experimentally observed with the measurements of the Nb film, can be qualitatively explained by the presence of a structured surface on the micrometric scale (the metamaterial itself) that alters the behavior and the vortex formation [33] leading, in the case of the metasurface, to a different evolution of the surface impedance as a function of the applied magnetic field.

3. Ultrastrong coupling with superconducting metasurface

Now we consider the complete system and we analyze the measurements where the superconducting metasurface is strongly coupled to the Landau levels of the 2DEG: we use a triangular quantum well in the GaAs/AlGaAs material system of sheet carrier density $\rho_{2DEG} = 3.2 \times 10^{11}\,\mathrm{cm}^{-2}$ (measured with Hall bars) with the channel lying 100 nm below the surface, already described in [17, 18]. An example of the inter-Landau level transition, or cyclotron resonance, that we observe from the triangular 2DEG without any metasurface is reported in figure 4(a).

The resonator we use also displays field enhancement in the TM polarization (electric field perpendicular to the semiconductor surface), which has been used to observe light-matter coupling with intersubband transitions [34]. From measurements (not shown) of the 2DEG alone in a tilted magnetic field [35] we deduce an energy separation between the first two subbbands of our triangular quantum well of at least 3 THz, so the ISB does not couple to the TM field of our resonator for the LC mode.

In figure 4(b) is visible a color plot of a transmission experiment carried out at 2.9 K. A clear anticrossing between the upper and lower branch is observed and we can measure a normalized coupling ratio $\frac{\Omega}{\omega} = 0.27$, which proves that the system is operating in the ultrastrong light-matter coupling regime. Due to the use of a complementary metasurface, the polaritonic branches are especially clear because the cyclotron signal gets filtered out. A transmission maximum parallel to the cyclotron dispersion is observable, starting from 1.4 T and a frequency of 0.5 THz, and is due to the coupling of the second mode of the resonator to the cyclotron resonance. We can then model the complete system using, as cavity parameters, the ones obtained with the measurements described in the previous paragraph and labeled as 'R_s MM' and 'X_s MM'. As visible from the color plot of figure 4(c), the experimental data is well reproduced by the numerical modeling. For convenience, the transmission peaks deduced from the simulations have been reported on the experimental data of figure 4(b) as black circles. The model is also able to reproduce weak features such as the coupling with the second mode of the cavity which is clearly visible as a weak maximum of transmission both in the direct measurements and in the simulation.

The 2DEG can be experimentally characterized by a complex conductivity, measured again by THz-TDS as in [36]. From the conductivity σ_{2DEG} we can deduce the frequency-dependent complex dielectric constant $\varepsilon = \varepsilon_\infty + \frac{i\sigma_{2DEG}}{\epsilon_0 \omega L_{eff}}$. Such an expression can be used to perform finite element simulations and contains all the physics of the system in a semiclassical description. The 2DEG is modeled by having an effective thickness $L_{eff} = 200\,nm$ (the value

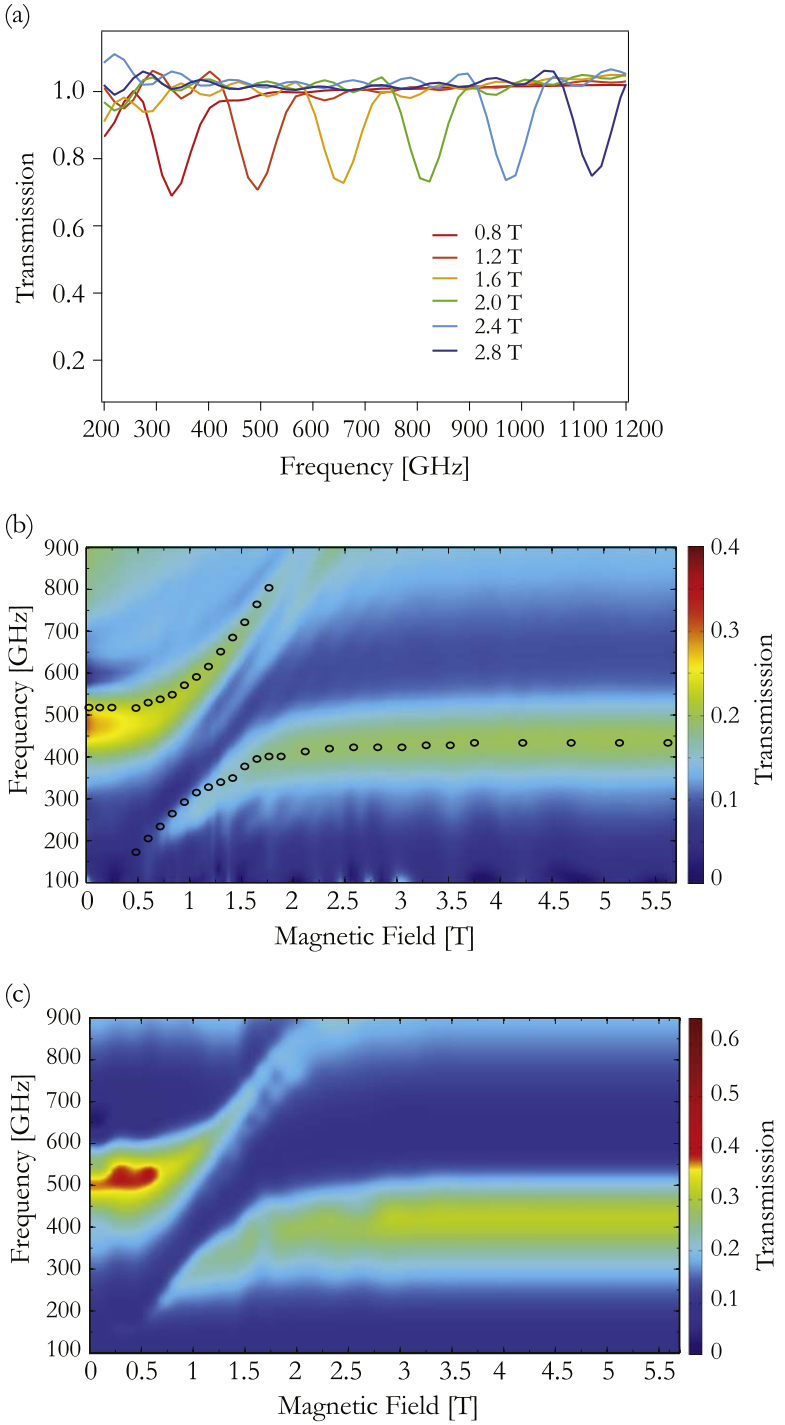

Figure 4. (a) Cyclotron absorption from the triangular well 2DEG for different values of the applied magnetic fields at a temperature of 2.9 K. (b) Transmission color plot for the Nb metasurface deposited on top of the triangular well 2DEG as a function of the applied magnetic field at T = 2.9 K. The black circles are the transmission maxima extracted from the numerical simulation of panel (c). (c) Simulated sample transmission as a function of the applied magnetic field for $T < T_c$.

resulting from band structure calculations is 20 nm, which leads to very long computation times of the 3D FE solver). We used the gyrotropic dispersion model of CST for a magnetized plasma.

As already observed in our previous experiments [17, 18], the bare resonator frequency ω_0 is blue-shifted to $\omega_0 + \Delta\omega$ when the cavity is loaded with the 2DEG electrons which are free to move in the x-y plane when no magnetic field is applied. The magnitude of the shift is directly related to the normalized coupling strength and is due to the quadratic terms of the light-matter Hamiltonian [4, 14]. As discussed also in [9–11, 37] the presence of this polaritonic gap is a signature of the ultrastrong light-matter coupling regime. We consider the expressions for the upper polaritonic branch $UP(B)$ and lower polaritonic branch $LP(B)$ derived from the theory of [14] and then we take the limits $\lim_{B\to+\infty} LP(B) = \omega_0$ and $\lim_{B\to 0} UP(B) = \omega_0 + \Delta\omega$. By a little algebra we obtain the following equation that relates the normalized light-matter coupling ratio $\frac{\Omega}{\omega_c}$ to the normalized frequency gap $\frac{\Delta\omega}{\omega_0}$:

$$\frac{\Omega}{\omega_c} = \frac{1}{2}\sqrt{\left(\frac{\Delta\omega}{\omega_0} + 1\right)^2 - 1}\,. \tag{4}$$

If we take the experimental values of the shift of the resonance frequency at B = 0 T ($\omega_{B=0}$ = 480 GHz) and at B = 6 T ($\omega_{B=6\,T}$ = 420 GHz) and we compute the expected light-matter coupling ratio, we find 0.28 which is in excellent agreement with the value 0.27 directly deduced from the anticrossing splitting 2Ω. We notice that the shift $\Delta\omega$ is also quantitatively reproduced by the finite element model. This happens because the conductivity model used for the 2DEG also yields the correct description for $B \to 0$, where the dielectric constant value is lowered by the free carrier contribution, which generates the blue shift of the cavity mode observed at B = 0. On the other limit, for high values of the magnetic field, the cavity resonant frequency assumes the value measured on the control sample (SI GaAs substrate), where no free electrons are present. It is remarkable that, in principle, we have a quantitative determination of the normalized coupling ratio even without applying any magnetic field. By looking at the frequency shift of the loaded cavity with respect to a reference, we can then apply equation (4) and obtain the value of the normalized ratio $\frac{\Omega}{\omega_c}$.

The value of the light-matter coupling ratio is independent from the material used to fabricate the cavities as it depends only on the geometry of the metamaterial elements. We performed similar strong coupling measurements on standard Au complementary cavities of identical design on the same heterostructure and we obtained $\frac{\Omega}{\omega_c} = 0.27$, in excellent agreement with what was found with Nb cavities. The cavity design of the present work is the complementary version of what was published by us in [18]: in that case the normalized coupling ratio was slightly higher ($\frac{\Omega}{\omega_c} = 0.34$) because the volume of the cavity for the direct metasurface was smaller, as was the mode extension in the growth direction which affects the coupling strength (see equation (2). A more detailed comparison among direct and complementary metamaterials in the ultrastrong coupling regime will be carried out elsewhere [38].

The possibility to modulate the ultrastrong coupling regime by changing the characteristics of the cavity is demonstrated in figure 5(a) where we show a series of transmission spectra taken at the anticrossing field B = 1.05 T by changing the sample's temperature from below to above T_c.

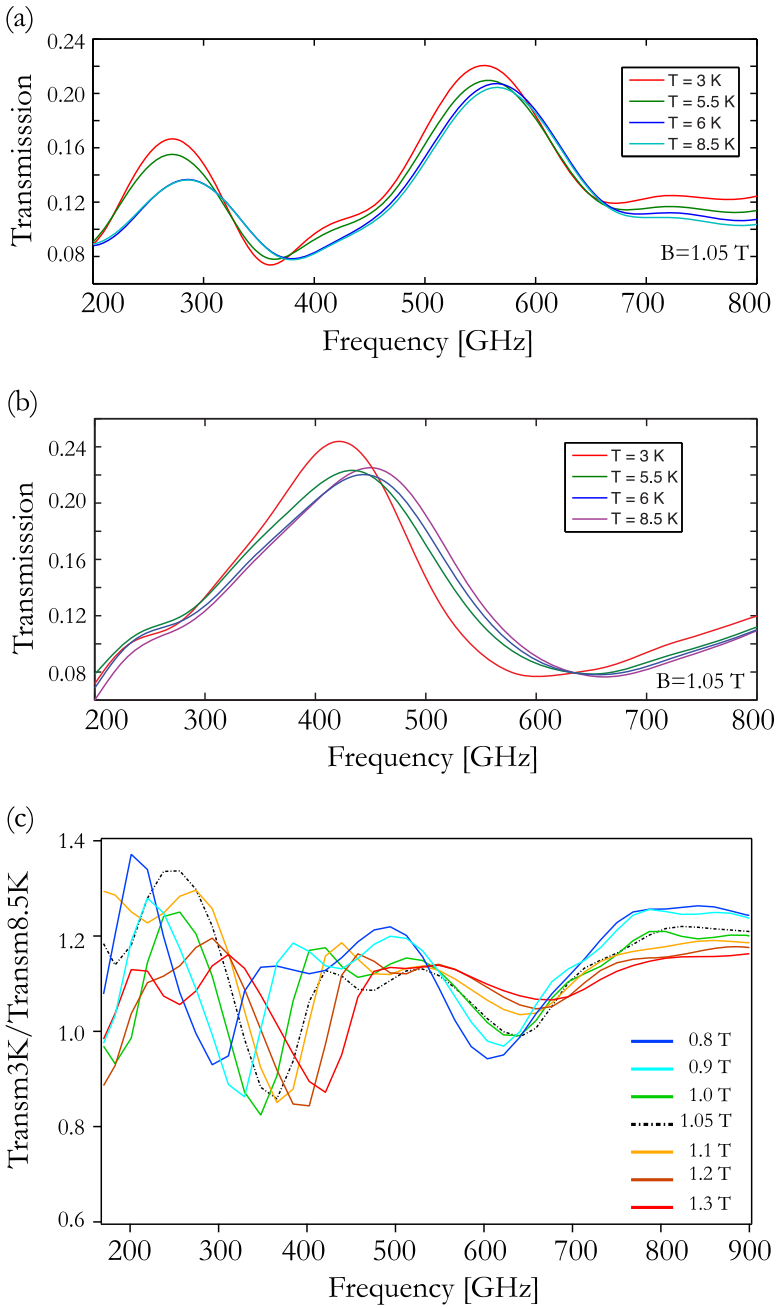

Figure 5. (a) Sample transmission at the anticrossing field of 1.05 T as a function of temperature. (b) Transmission for the super conducing metasurface deposited on SI GaAs. (c) Ratio between transmittance spectra at 3 K and 8.5 K for different magnetic fields ranging from 0.8 T to 1.3 T.

We can clearly observe a modulation both in intensity and in frequency of both polariton peaks, which reflects what was observed in the same conditions for the reference sample with Nb on SI GaAs, reported in figure 5(b). In order to better analyze the impact of the superconducting transition on the ultrastrongly coupled system, we plot in figure 5(c) the ratio between the transmission spectra at 3 K and the ones at 8.5 K for magnetic fields values in the

range 0.8–1.3 T. We consider 8.5 K because, as visible from figure 5(b), the superconducting transition at 1.05 T has already taken place between 5.5 and 6 K. As visible from the graph, the relative change of both polaritonic branches is significant, reaching 35% for the lower branch and 20% for the upper branch. It is interesting to note the different behavior of the lower and upper branches as a function of the applied field. The relative change for the upper branch steadily decreases to zero while the magnetic field is increased. On the contrary, the relative change of the lower branch reaches a maximum for the resonant value of B = 1.05 T but never goes below 15 % in the range of magnetic fields 0.8–1.3 T. This can be explained by the fact that the upper branch becomes more and more matter-like and then the impact of the temperature change is much weaker compared to the cavity. The lower branch, on the contrary, becomes more cavity-like and thus is more affected by the cavity change.

4. Conclusions

In conclusion, we presented light-matter coupling experiments in the THz range employing complementary superconducting metasurfaces. The system operates in the ultrastrong coupling regime and the presence of the superconducting cavity allows the modulation of the resonant frequency and of the quality factor of the resonator. As already shown in literature, the superconducting metasurface can be modulated in an ultrafast way, on a sub-picosecond timescale [39, 40]. In future work we will leverage on this aspect and realize non-adiabatic experiments in the ultrastrong coupling regime in our magnetopolaritonic system.

Acknowledgments

This research was supported by the Swiss National Science Foundation (SNF) through the National Centre of Competence in Research Quantum Science and Technology and through the SNF grant no. 129823. GS would like to acknowledge F Chiarello for discussions.

References

[1] Haroche S and Raimond J 2006 *Exploring the Quantum* (Oxford University Press)
[2] Raimond J, Brune M and Haroche S 2001 *Rev. Mod. Phys.* **73** 565
[3] Wallraff A *et al* 2004 *Nature* **431** 162
[4] Ciuti C, Bastard G and Carusotto I 2005 *Phys. Rev.* B **72** 115303
[5] Niemczyk T *et al* 2010 *Nature Physics* **6** 772
[6] Bloch F and Siegert A 1940 *Phys. Rev.* **57** 522
[7] Anappara A *et al* 2009 *Phys. Rev.* B **79** 201303
[8] Guenter G *et al* 2009 *Nature* **458** 178
[9] Delteil A *et al* 2012 *Phys. Rev. Lett.* **109** 246808
[10] Geiser M *et al* 2012 *Phys. Rev. Lett.* **108** 106402
[11] Todorov Y *et al* 2010 *Phys. Rev. Lett.* **105** 196402
[12] Muravev V M, Gusikhin P A, Andreev I V and Kukushkin I V 2013 *Phys. Rev.* B **87** 045307
[13] Devoret M H, Girvin S M and Schoelkopf R J 2007 *Ann. Phys., Lpz.* **16** 767
[14] Hagenmüller D, De Liberato S and Ciuti C 2010 *Phys. Rev.* B **81** 235303
[15] Carter S *et al* 2005 *Science* **310** 651

[16] Zaks B *et al* 2011 *New J. Phys.* **13** 083009
[17] Scalari G *et al* 2012 *Science* **335** 1323
[18] Scalari G *et al* 2013 *J. Appl. Phys.* **113** 136510
[19] Wilson C M *et al* 2011 *Nature* **479** 376
[20] Ridolfo A, Savasta S and Hartmann M J 2013 *Phys. Rev. Lett.* **110** 163601
[21] Ridolfo A, Vilardi R, Stefano O D, Portolan S and Savasta S 2011 *Phys. Rev. Lett.* **106** 013601
[22] Stassi R, Ridolfo A, Stefano O D, Hartmann M J and Savasta S 2013 *Phys. Rev. Lett.* **110** 243601
[23] Falcone F *et al* 2004 *Phys. Rev. Lett.* **93** 197401
[24] Chen H-T *et al* 2007 *Optics Express* **15** 1084
[25] Ricci M, Orloff N and Anlage S M 2005 *Appl. Phys. Lett.* **87** 034102
[26] Jin B *et al* 2010 *Optics Express* **18** 17504
[27] Zhang C H *et al* 2012 *Optics Express* **20** 42
[28] Chen H-T *et al* 2010 *Phys. Rev. Lett.* **105** 247402
[29] Pronin A V *et al* 1998 *Phys. Rev.* B **57** 14416
[30] Tinkham M 1996 *Introduction to Superconductivity* 2nd edn (New York: Dover)
[31] Bardeen J and Stephen M J 1965 *Phys. Rev.* **140** A1197
[32] Ricci M 2007 *PhD Thesis* University of Maryland
[33] Baert M, Metlushko V V, Jonckheere R, Moshchalkov V V and Bruynseraede Y 1995 *Phys. Rev. Lett.* **74** 3269
[34] Dietze D, Benz A, Strasser G, Unterrainer K and Darmo J 2011 *Optics Express* **19** 13700
[35] Schlesinger Z, Hwang J C M and Allen S J 1983 *Phys. Rev. Lett.* **50** 2098
[36] Wang X *et al* 2007 *Optics Letters* **13** 1845
[37] Todorov Y and Sirtori C 2012 *Phys. Rev.* B **85** 045304
[38] Maissen C *et al* 2014 unpublished
[39] Singh R *et al* 2012 *Nanophotonics* **1** 117
[40] Beck M *et al* 2011 *Phys. Rev. Lett.* **107** 177007